EXPANSION PROCESSES AND STRUCTURES OF TWO-PHASE FLOWS IN AERATED-LIQUID JETS DISCHARGED INTO A QUIESCENT ENVIRONMENT

KUO-CHENG LIN[1], ALAN KASTENGREN[2] & CAMPBELL CARTER[3]
[1]Taitech, Inc., USA
[2]Argonne National Laboratory, USA
[3]Air Force Research Laboratory, USA

ABSTRACT

Expansion processes and near-field structures in the two-phase flow within an aerated-liquid jet injected into a quiescent environment were experimentally explored with the confocal x-ray fluorescence technique available at Argonne National Laboratory. Quantitative time-averaged liquid and gas density distributions within the aerated-liquid jet were spatially resolved simultaneously. For the present injection condition, the observation of a dome-shaped gas plume head and a high gas density gradient within a short distance from the nozzle exit clearly indicates that the initial gas expansion processes across the nozzle exit are highly similar to those within a typical under-expanded gaseous jet. With the assistance of compressible gas expansion near the nozzle exit, the liquid plume exhibits a plume width larger than that of the aerating gas plume, leading to a separation between liquid and gas plumes at the downstream location. Expansion of the gas plume creates a region of low gas density, followed by a region of gas density recovery in the near field. The low gas density region resembles the region with over-expanded gas in front of a Mach disk inside a typical under-expanded gaseous jet. The density variation within the low density region, however, is small, indicating a low level of over expansion and a weak Mach disk. The present analysis of Mach disk location within the discharged aerating gas plume shows that, while the location can be generally identified from gas density measurements, the use of correlations for location identification may be unreasonable, due to the lack of direct measurement data on characteristic pressures.

Keywords: two-phase flow, aerated-liquid jet, confocal x-ray fluorescence, under-expanded gaseous jet.

1 INTRODUCTION

Two-phase flow generation and handling are of great interest in applications in the petroleum, civil, chemical, nuclear, propulsion, and power industries. For instance, liquid (or effervescent, or barbotage) aeration is a plausible scheme to enhance liquid atomization for painting, agriculture sprays, or propulsion/power systems [1]. By creating a two-phase mixture inside an aerated-liquid injector using a small amount of gas mixed with the liquid fuel, the liquid atomization processes can be greatly accelerated, for the generation of a well-dispersed plume for effective mixing with the ambient air and, therefore, for efficient combustion [2], [3]. Successful characterization of structures and expansion processes in the two-phase flow discharged from an aerated-liquid injector or other device can greatly advance these applications.

In order to better characterize the discharged two-phase flow, which is compressible and can be optically dense, capable in-situ diagnostic techniques are required. Recently, two-phase flow structures of aerated-liquid jets have been successfully explored with various x-ray diagnostic techniques, including high-speed x-ray phase contrast imaging (PCI), x-ray radiography, and x-ray fluorescence [4]–[7]. In particular, the study of Lin et al. [7] utilized the x-ray fluorescence technique to quantitatively characterize the line-of-sight (*LOS*) liquid and gas mass distributions within the discharged aerated-liquid jets. For the injection

condition with a high injection pressure, the discharged two-phase flows exhibit gas-jet-like expansion processes in the aerating gas. In addition, the gas plume is narrower than the liquid plume. The expansion processes, however, were not further explored.

The capability of x-ray diagnostics to characterize the structures of an under-expanded argon gas jet was demonstrated in the study of Scarcelli et al. [8]. The Mach disk location was clearly identified from the *LOS* gas density contours, using x-ray radiography. This approach to identify the possible shock structure within a two-phase jet can, however, be problematic, due to the liquid, which has high x-ray absorbance within the line of sight.

The confocal x-ray fluorescence technique was recently applied by Lin et al. [9] to spatially resolve both liquid and gas mass distributions within discharged aerated-liquid jets. Quantitative cross-sectional mass distribution contours were obtained at several axial locations in a quiescent environment. The phenomenon of a narrower gas plume persisting inside the liquid plume was confirmed. No efforts were made, however, to spatially resolve shock structures within the aerated-liquid jet.

The objective of the present study is to use the confocal x-ray fluorescence technique to spatially resolve both liquid and gas mass distributions, with emphasis on exploring the expansion processes within the near field of an aerated-liquid jet.

2 EXPERIMENTAL METHODS

2.1 Injector assembly

The experiment was conducted at the 7-BM beamline of the Advanced Photon Source (APS) at Argonne National Laboratory. For the present study, the discharged spray was placed in the path of a focused x-ray beam. Liquid and aerating gas were supplied into the aerated-liquid injector at the desired flow rates to form a two-phase mixture inside the injector before discharge into a quiescent environment. The aerated-liquid injector features the *outside-in* aeration configuration, with the aerating gas flowing through an annular passage before entering the central liquid stream for mixing. Fig. 1(a) shows a schematic of the injection assembly, which has a stainless steel injector body, an aerating tube, and an exchangeable beryllium nozzle. The aerating tube has an internal diameter of 2.2 mm and features 32 small orifices located in 16 rows with two 0.18 mm diameter orifices in each row, as shown in Fig. 1(b). Orifices in each row are offset by 90 degrees from the orifices in adjacent rows,
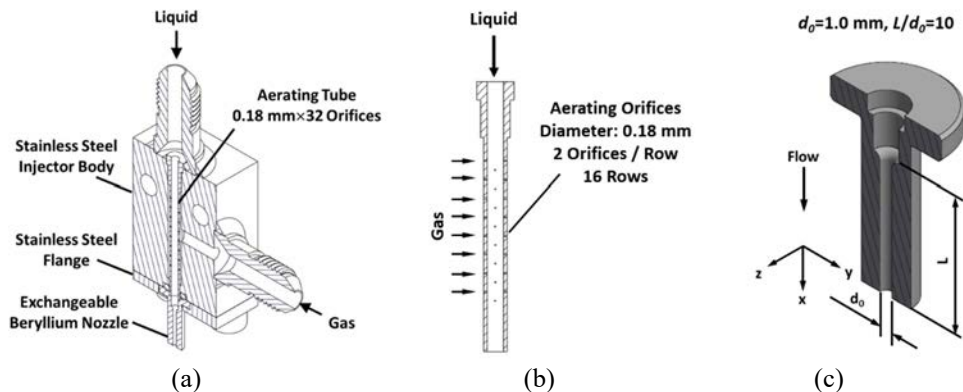

Figure 1: Schematics of (a) Aerated-liquid injector body; (b) Aerating tube; and (c) Beryllium nozzle.

resulting in an orifice distribution pattern in four columns on the aerating tube. The beryllium nozzle used for the present study features a contoured entrance, followed by a cylindrical passage with a constant diameter (d_0) of 1.0 mm and passage length (L) of 10 mm, and thus an L/d_0 of 10. The nozzle connects smoothly with the aerating tube via a short plenum section with a diameter of 2.2 mm. A schematic of this nozzle is shown in Fig. 1(c).

The aerated-liquid jet was discharged vertically into a collecting bucket with a small opening on the cap to minimize the probability of stray droplets entering the beam path. The distance between the nozzle exit and the bucket cap was kept around 5 mm, in order to allow probing of the discharged jet and at the same time avoid splashing. Both the aerated-liquid injector and the collecting bucket were rigidly mounted on a traversing table, which provided movement normal to the x-ray beam.

For the present study, the injection condition consists of a liquid flow rate, m_L, of 18.2 g/s and a gas-to-liquid mass ratio, GLR, of 6.72%. The injection pressures (P_{inj}) and temperatures (T_{inj}) measured just upstream of the injector assembly were 3.69 MPa and 294 K, respectively. The ambient is at atmospheric pressure. At this injection condition with a relatively large P_{inj}/P_∞ of 36.5, the discharged plume is highly dispersed with a fairly large plume width for x-ray probing.

2.2 X-ray measurements

The 7-BM beamline at Argonne National Laboratory is dedicated to ultrafast x-ray radiography, fluorescence, and tomography experiments in fuel sprays and associated phenomena. The x-ray source for the beamline is a synchrotron bending magnet, which produces nearly collimated, broadband x-ray emission. The beamline consists of two radiation enclosures. The first enclosure (7-BM-A) houses a pair of slits to limit the x-ray beam size and a double multilayer monochromator (1.2–4.3% ΔE/E) to filter the beam. The resulting monochromatic beam then passes into the second radiation enclosure (7-BM-B), which houses the experimental equipment. More information regarding the beamline performance can be found in [10].

Fluorescence of x-rays from tracer elements in the liquid and gas is caused by the relaxation of atoms to a more stable state after the ionization of a core-shell electron due to absorption of an incident x-ray photon. The energy of the emitted photons is characteristic of the atomic number of the atoms emitting the photons, and the emitted fluorescence flux is proportional to the amount of fluorescent material in the beam. X-ray fluorescence is commonly used for nondestructive elemental analysis. More detail of the x-ray fluorescence process is given in [11] and [12].

Here, x-ray fluorescence was used to simultaneously measure gas and liquid concentrations in the spray. X-ray fluorescence from the liquid and gas phases can be used to determine the distributions of liquid and gas independently, by doping the working fluids with bromine (Br) and krypton (Kr) atoms, respectively. Sodium bromide ($NaBr$) was dissolved into the water at a concentration of 0.42% by mass. This concentration was monitored during the experiment by measuring the electrical conductivity of the water, which was approximately 4.5 mS/cm. The gas phase was pre-mixed (by the gas vendor) to a concentration of 6% Kr (and 94% N_2) by volume. For the current x-ray fluorescence experiments, the mean x-ray beam photon energy was set at 15 keV; a photon energy of at least 14.3 keV is required to excite both Br and Kr. The beam was focused using a pair of 300 mm long Kirkpatrick–Baez focusing mirrors. The beam focus is approximately 5×6 μm FWHM V × H, located approximately 500 mm from the center of the horizontal focusing mirror. The effective size of the beam for the current sprays (which are several mm wide) is

somewhat greater than this minimum focus size. The experimental setup at the 7-BM beamline is shown schematically in Fig. 2.

The fluorescence photons emitting from the media of interest within the focused probe volume were collected by a polycapillary x-ray optic and then measured by a silicon drift diode detector. Fig. 3 shows the present x-ray fluorescence test section setup. The polycapillary x-ray optic has a focal length of 50 mm and a spatial resolution of approximately 200 μm at the Br and Kr fluorescence photon energies, and it was placed in front of the fluorescence detector to filter out all x-rays but those originating from the focal region. The integrated detector assembly was then positioned at 90° relative to the x-ray beam in the horizontal plane to minimize the scattering detected by the detector. The effective probe volume for the present measurements is defined by the focused beam size and the focal spot size of the polycapillary optic: $5 \times 6 \times 200$ μm. With this small probe volume, distributions of liquid and gas mass can be resolved in three dimensions by moving the spray normal to the x-ray beam and the detector and polycapillary together along the x-ray beam.
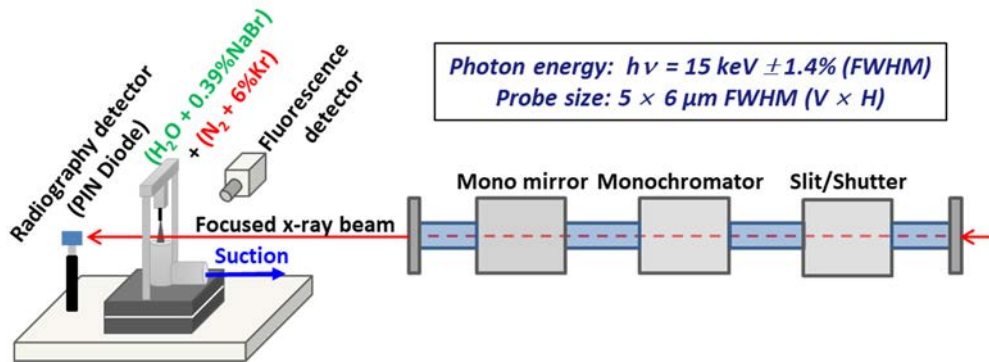

Figure 2: X-ray and injection stand setup at the 7-BM beamline at the Argonne National Laboratory.
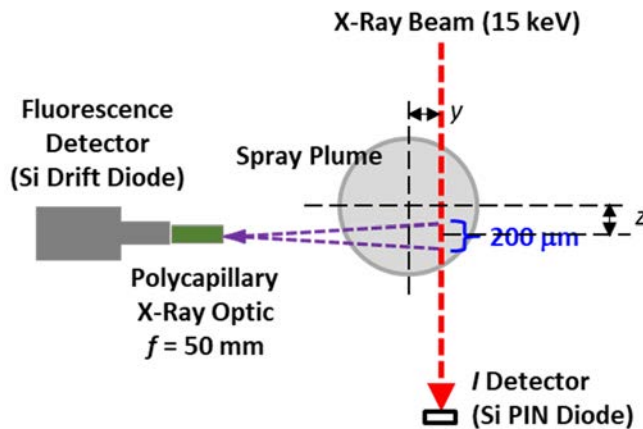

Figure 3: Confocal x-ray fluorescence setup.

The measurement was carried out within the near field of the discharged plume (less than 3.0 mm from the nozzle exit plane, i.e., $x < 3.0$ mm; $x = 0$ at the nozzle exit) with prescribed probing locations within a center sliced plane (x-y plane, y in the transverse direction relative to the injector axis). Calibration scans at known liquid and gas densities were carried out to quantitatively correlate the measured signal to local densities.

3 RESULTS AND DISCUSSION

3.1 Two-phase flow structures

Fig. 4 shows the cross-sectional liquid and gas density contours within the near field of the discharged plume. Please note that in contrast to the previous x-ray fluorescence measurements in the study of Lin et al. [7], the current data are not pathlength integrated. Instead, these data truly represent a cross-sectional slice of the fluid distribution. The liquid density contours exhibit an annular-like liquid distribution pattern near the nozzle exit plane, with the most upstream measurement location being $x = 0.1$ mm. This observation clearly indicates that more liquid stays close to the nozzle passage wall before discharge for the present injection condition. A smaller amount of liquid is distributed in the core region of the two-phase mixture within the nozzle passage and the discharged plume at $x < 0.6$ mm. The discharged liquid is quickly dispersed as the flow progresses downstream, with no distinct annular liquid distribution pattern in the downstream locations ($x > 0.6$ mm).
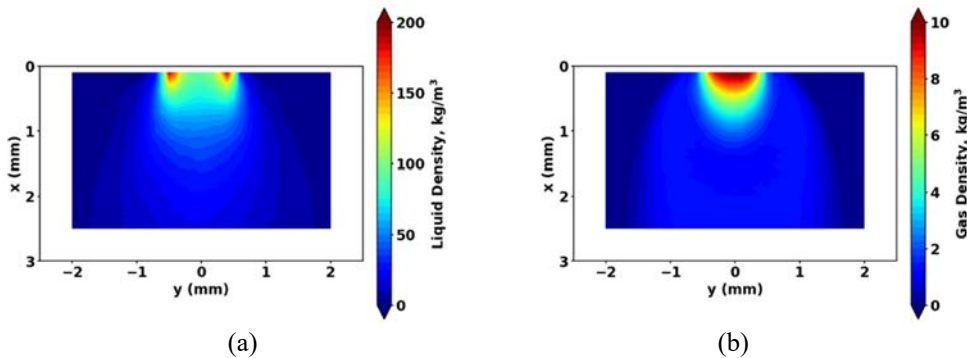

Figure 4: Cross-sectional (a) Liquid; and (b) Gas density contours in linear scale within the near field of the discharged plume. Injector exit plane at $x = 0$ and injector axis at $y = 0$.

The discharged aerating gas exhibits a dome-shaped region of high density within the near field. The high-density gas quickly expands to a low value within a short distance of $x < 1.2$ mm from the nozzle exit. It appears that the present injection condition with a relatively large (P_{inj}/P_∞) of 36.5 exhibits a gas plume structure similar to that of a highly under-expanded gaseous jet. Unlike in the study of Scarcelli et al. [8], however, the typical features of an under-expanded gaseous jet, such as the presence of barrel shock and Mach disk, cannot be observed in the present planar gas density contours.

A gaseous jet injected from a sonic nozzle into a quiescent environment can be classified as subsonic, moderate under-expanded, or highly under-expanded jet, depending on the (P_0/P_∞) value of the injection condition, where P_0 is the stagnation pressure in the plenum of

the nozzle. Based on the study of Donaldson and Snedeker [13], the range of (P_0/P_∞) values for each type of discharged gaseous jet for air is listed in Table 1. Also listed in the table is the range of (P_{exit}/P_∞) values for each type of discharge jet, where P_{exit} is the local pressure at the nozzle exit. The large (P_{inj}/P_∞) value of 36.5 for the present injection condition indicates that the aerating gas jet is highly under-expanded.

Table 1:   Ranges of (P_0/P_∞) and (P_{exit}/P_∞) values for three major variations of gaseous jets discharged from a sonic nozzle into a quiescent environment. *(Source: Donaldson and Snedeker [13].)*

Subsonic jet	Moderate under-expanded jet	Highly under-expanded jet
$1 < P_0/P_\infty < 1.89$	$2.08 < P_0/P_\infty \leq 3.85$	$P_0/P_\infty > 3.85$
$P_{exit}/P_\infty = 1$	$1.1 < P_{exit}/P_\infty \leq 2$	$P_{exit}/P_\infty > 2$

It should be noted that the use of the measured injection pressure, P_{inj}, to present the stagnation pressure, P_0, for the purposes of jet structure classification may be problematic, due to pressure losses during the mixing of liquid and aerating gas within the injector. In addition, the presence of liquid within the gas plume of an aerated-liquid jet may affect the gas expansion processes. Nonetheless, the aerating gas jet seen here exhibits a certain degree of under-expansion, as evidenced by the dome-shaped plume head and a rapid decrease in gas density within a short distance.

Fig. 5 shows the density contours from Fig. 4 plotted in logarithmic scale, in order to enhance the differentiation in the mass distributions. The liquid plume structure is affected by the compressible gas plume. The most pronounced effect takes place right at the nozzle exit, where the initial expansion of the aerating gas pushes liquid rapidly outward in the transverse direction, resulting in a large initial spreading angle for the liquid plume. The aerating gas plume exhibits a dome-shaped plume head to constrain the spreading rate in plume width. The liquid plume, however, is not affected by the change in gas plume shape and exhibits a constant spreading rate within the field of view. Consequently, the outer edge of the liquid plume quickly separates from that of the aerating gas plume. The liquid plume width is larger than that of the aerating gas plume. The narrow gas plume stays within the liquid plume at the end of the probing area.

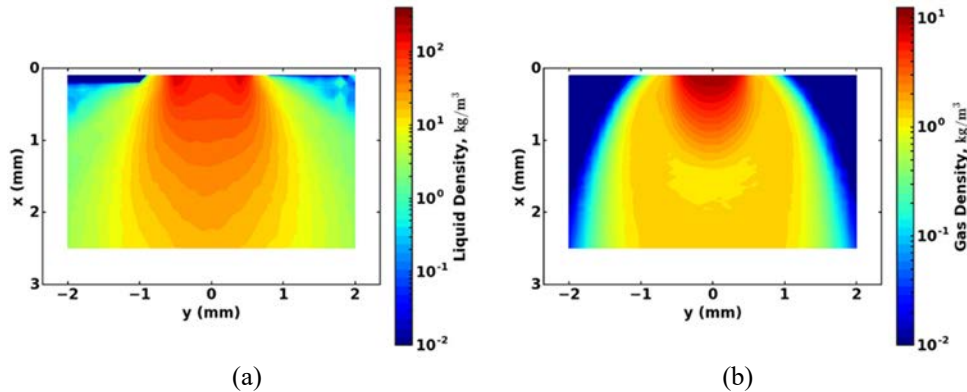(a)   (b)

Figure 5:   Cross-sectional (a) Liquid; and (b) Gas density contours in logarithmic scale within the near field of the discharged plume.

In the gas density contours, a region with a noticeably low gas density can be observed between $x = 1.4$ and 2.0 mm, indicating a small degree of over expansion within the aerating gas plume. The slightly over-expanded gas density recovers within a short distance. This observation is similar to the phenomenon associated with pressure rise across a Mach disk in a typical under-expanded gaseous jet.

Fig. 6 shows the radial distribution profiles of liquid and gas densities at selected axial locations. The liquid distribution exhibits an annular-like profile at both $x = 0.1$ and 0.4 mm locations. The annular liquid distribution pattern quickly transitions to a Gaussian distribution pattern around $x = 0.5$ mm. The radial distribution profiles of gas density exhibit a quick reduction within a short distance ($x < 1.2$ mm), followed by a fairly constant distribution pattern with a gradual increase in plume width. A region with a noticeably low gas density (on a linear scale) can be observed around the $x = 1.5$ mm location, indicating a slight gas over expansion, followed by a recovery, as described earlier.
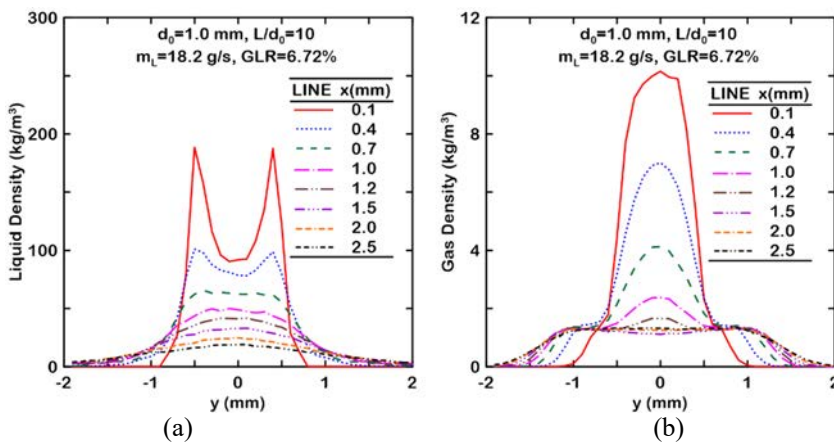

Figure 6:   Radial distribution profiles for (a) Liquid; and (b) Gas densities at selected axial locations.

Fig. 7 shows the axial distribution profiles for liquid and gas densities in linear and logarithmic scales, respectively. The axial liquid density profile decreases continuously from the nozzle exit within the present probing range. The axial gas density profile also exhibits a rapid decrease initially and, with the use of logarithmic scale, reaches a density lower than the ambient gas density of around 1.18 kg/m^3 (as shown in Fig. 7(b)), followed by a gradual recovery to a gas density of 1.32 kg/m^3 at the end of the present probing range. This gas density recovery is not as dramatic as the recovery processes across a Mach disk within a typical under-expanded gaseous jet. It seems that a weak Mach disk or compression wave(s) exists within the present discharged aerating gas jet; the unique features of gas over-expansion and density recovery indicate that the discharged aerating gas jet in the present injection condition weakly resembles an under-expanded gaseous jet.

The presence of liquid phase within the aerating gas plume of the present aerated-liquid jet may greatly affect the expansion processes, retarding the gas expansion processes and limiting gas density variation. The liquid phase may also disrupt shock wave formation at a particular spatial location, rendering the identification of a shock wave in the present time-averaged measurements uncertain or even impossible.
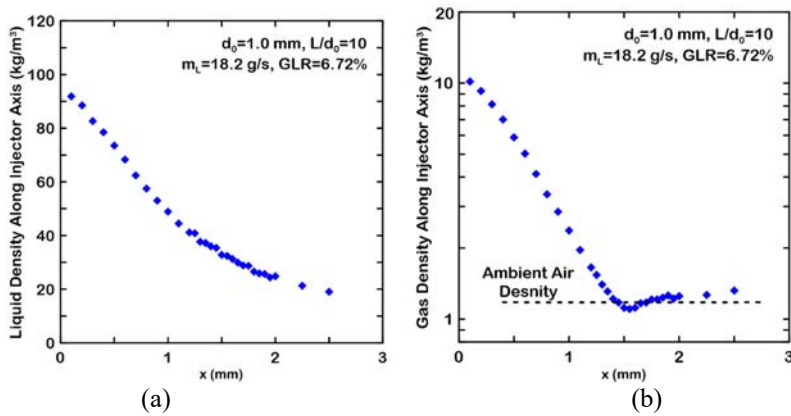
Figure 7:   Axial distribution profiles for (a) Liquid (in linear scale); and (b) Gas (in logarithmic scale) densities.

3.2 Further examination of gas plume structures

The characteristics of a discharged aerated-liquid jet, such as mass distribution profiles, plume width, and plume spreading angle, depend on the two-phase flow structures inside the injector and the subsequent expansion processes of the near-field plume. The present measurements have shown that the initial expansion processes of the discharged liquid are greatly affected by the expansion of the compressible aerating gas. In particular, the aerating gas plume in the near field exhibits features highly similar to a typical under-expanded gaseous jet. If a Mach disk does exist inside the discharged aerating gas plume (even though not identified in the present measurements), it is possible that its location could be predicted from correlations that were developed for predicting Mach disk location within an under-expanded gaseous jet.

Two correlations for the prediction of Mach disk location inside a typical under-expanded gaseous jet, one by Crist et al. [14], and the other by Lewis and Carlson [15], are explored here, along with a correlation for Mach disk diameter by Addy [16]. The correlation of Crist et al. [14] is based on the (P_0/P_∞) ratio, as follows:

$$\frac{x_{MD}}{d_0} = \sqrt{\frac{\left(\frac{P_0}{P_\infty}\right)}{2.4}} = 0.6455 \times \sqrt{\frac{P_0}{P_\infty}}. \tag{1}$$

The parameter x_{MD} is the Mach disk location measured from the nozzle exit. Please note that eqn (1) is independent of gas type or the specific heat ratio (γ) and is a function of the (P_0/P_∞) ratio. It can be readily applied to an under-expanded gaseous jet undergoing an isentropic expansion process. The direct use of P_{inj} to replace P_0 in eqn (1) gives a predicted Mach disk location of $x_{MD} = 3.9$ mm. This predicted value does not agree with the location of gas density recovery illustrated in Fig. 7(b) and places the Mach disk downstream of the present probing range.

As noted previously, however, it is highly problematic to treat the formation of two-phase mixtures within the aerated-liquid injector as an isentropic process, given pressure losses during the mixing of liquid and aerating gas within the injector. If the Mach disk location is

defined as the location where the axial gas density rise from the minimum value intersects with the levelled-off density value, the gradual density recovery in Fig. 7(b) prevents an unambiguous identification of the Mach disk location for the present aerating gas plume. For assessment purposes, therefore, the Mach disk is estimated at the x_{MD} = 1.75 mm location. With this measurement, the effective stagnation pressure, $P_{0,eff}$, which is defined as the stagnation pressure for the present gas plume to generate a Mach disk location from eqn (1) to perfectly match the measurement, is 0.72 MPa. The derived $P_{0,eff}$ is about 20% of the present P_{inj} value. The differences between P_{inj} and $P_{0,eff}$ can be treated as the pressure losses associated with the injector design and the mixing between liquid and aerating gas. Based on the classification criteria with (P_o/P_∞) in Table 1, the present ($P_{o,eff}/P_\infty$) value of 7.1 indicates that the aerating gas jet is highly under-expanded for the present Mach disk location measurement of x_{MD} = 1.75 mm.

A correlation for Mach disk diameter prediction was proposed by Addy [16], as follows:

$$\frac{d_{MD}}{d_0} = 0.31 \times \sqrt{\frac{P_0}{P_\infty} - 5}. \tag{2}$$

The parameter d_{MD} is the Mach disk diameter. The use of the present ($P_{o,eff}/P_\infty$) value gives d_{MD} = 0.46 mm. Fig. 8 shows the gas density contour with measured and predicted locations and diameter of the Mach disk. The Mach disk diameter predicted using this correlation is significantly smaller than the measured gas plume width.
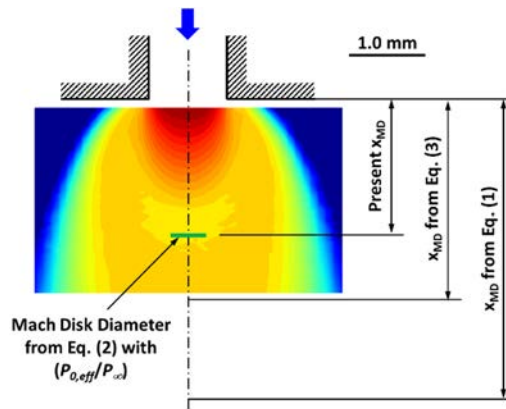

Figure 8:   Measured Mach disk location and predicted Mach disk locations and diameter from [14]–[16].

The second correlation for Mach disk location prediction is based on the (P_{exit}/P_∞) ratio of Lewis and Carlson [15], as follows:

$$\frac{x_{MD}}{d_0} = 0.69 \times M_{exit} \times \sqrt{\gamma \times \frac{P_{exit}}{P_\infty}}. \tag{3}$$

The parameter M_{exit} is the Mach number at the nozzle exit. In the present study, P_{exit} was not measured. Instead, the local pressures derived from x-ray fluorescence measurements in the study of Lin et al. [17] inside the same beryllium nozzle with the same injector assembly were used to estimate the P_{exit} value. Fig. 9 (from [17]) shows the local pressure profiles in

the axial direction inside the nozzle for the present injection condition. The value of P_{exit} was extrapolated from the third-order polynomial fitting of the derived local pressures. The study of Lin et al. [17] has also shown that the two-phase flows are choked at the nozzle exit, that is, $M_{exit} = 1.0$, mainly due to the reduction in the speed of sound for compressible two-phase mixtures. The present krypton/nitrogen mixture has a γ value of 1.409, which is similar to that of air (1.4).
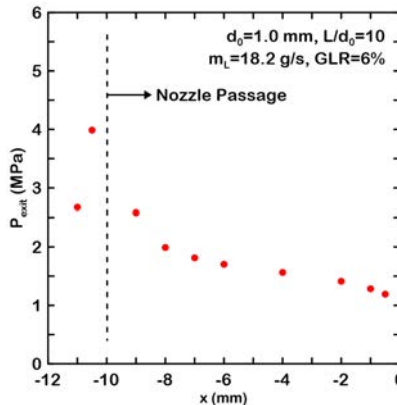

Figure 9: Local pressure within the nozzle section of an aerated-liquid injector. *(Source: Lin et al. [17].)*

With the extrapolated P_{exit} value of 1.08 MPa, the predicted Mach disk location from eqn (3) is $x_{MD} = 2.7$ mm, which is closer to the present measurements but still outside the present probing range, as is shown in Fig. 8. The use of P_{exit} excludes the pressure losses associated with the liquid/gas mixing processes upstream of the nozzle passage and may therefore be more representative of the local state of the two-phase mixture prior to discharge into the ambient. Eqn (3) can therefore be expected to provide a better prediction of the Mach disk location. The use of the derived P_{exit} value may, of course, carry over uncertainties from [17], and should be replaced by directly measured P_{exit} in the future. An effective exit pressure, $P_{exit,eff}$ – which is defined as the exit pressure for the present gas plume to generate a Mach disk location from eqn (3) to perfectly match the measurement – is 0.45 MPa. Table 2 summarizes the ratios between characteristic pressures and the ambient pressure. Based on the classification criteria with (P_{exit}/P_∞) in Table 1, both (P_{exit}/P_∞) value of 10.7 and $(P_{exit,eff}/P_\infty)$ value of 4.4 indicate that the aerating gas jet is also highly under-expanded.

Table 2: Measured and derived pressures and ratios with ambient pressure.

P_{inj}	$P_{0,eff}$	P_{exit}	$P_{exit,eff}$	P_{inj}/P_∞	$P_{0,eff}/P_\infty$	P_{exit}/P_∞	$P_{exit,eff}/P_\infty$
3.69 MPa	0.72 MPa	1.08 MPa	0.46 MPa	36.5	7.1	10.7	4.4

4 SUMMARY

Expansion processes and near-field structures of an aerated-liquid jet injected into a quiescent environment were experimentally explored with the confocal x-ray fluorescence technique available at Argonne National Laboratory. Quantitative time-averaged liquid and gas density

distributions within the aerated-liquid jet were spatially resolved simultaneously. The major conclusions of the present study are, as follows:

1. For the present injection condition, the observation of a dome-shaped gas plume head and a high gas density gradient within a short distance from the nozzle exit clearly indicate that the initial gas expansion processes across the nozzle exit are highly similar to those within a typical under-expanded gaseous jet.
2. With the assistance of compressible gas expansion near the nozzle exit, the liquid plume exhibits a plume width larger than that of the aerating gas plume, leading to a separation between liquid and gas plumes at the downstream location.
3. Expansion of the gas plume creates a region of low gas density, followed by a region of gas density recovery within the near field. The low gas density region resembles the region with over-expanded gas in front of a Mach disk inside a typical under-expanded gaseous jet. The density variation within the low density region, however, is small, indicating a low level of over expansion and a weak Mach disk.
4. The present analysis of Mach disk location within the discharged aerating gas plume shows that the location can be approximately identified from the present gas density measurements. The use of correlations from the literature to further pinpoint the location poses a significant challenge, due to the lack of direct measurements of characteristic pressures.

Accurate and relevant pressure measurements inside an aerated-liquid injector would greatly improve the understanding of the structures of aerated-liquid jets.

REFERENCES
[1] Lefebvre, A.H., Wang, X.F. & Martin, C.A., Spray characteristics of aerated-liquid pressure atomizers. *J. Propulsion Power*, **4**, pp. 293–298, 1988.
[2] Sovani, S.D., Sojka, P.E. & Lefebvre, A.H., Effervescent atomization. *Progress in Energy and Combustion Science*, **27**, pp. 483–521, 2001.
[3] Mathur, T. et al., Liquid JP-7 combustion in a scramjet combustor. *AIAA Paper 2000-3581*, 2000.
[4] Lin, K.-C., Rajnicek, C., McCall, J., Carter, C. & Fezzaa, K., Investigation of pure- and aerated-liquid jets using x-ray phase contrast imaging technique. *Nuclear Instruments and Methods in Physics Research Section A*, **649**(1), pp. 194–196, 2011.
[5] Lin, K.-C., Carter, C., Smith, S. & Kastengren, A., Exploration of aerated-liquid jets using x-ray radiography. *AIAA Paper 2012-0347*, 2012.
[6] Lin, K.-C., Carter, C., Smith, S. & Kastengren, A., Characterization of aerated-liquid jets using simultaneous x-ray radiography and x-ray fluorescence measurements. *Proceedings of the 26th Annual Conference on Liquid Atomization and Spray Systems*, 2014.

[7]   Lin. K.-C., Carter, C., Kastengren, A. & Peltier, S., Exploration of gas phase properties in aerated-liquid jets using x-ray fluorescence. *AIAA Paper 2015-0165*, 2015.

[8]   Scarcelli, R., Kastengren, A., Powell, C., Wallner, T. & Matthias, N., High-pressure gaseous injection: a comprehensive analysis of gas dynamics and mixing effects. *ASME Paper No. ICEF2012-92137*, pp. 793–801, 2012

[9]   Lin, K.-C., Kastengren, A. & Carter, C., Exploration of temporal and time-averaged two-phase flow structures using x-ray diagnostics. *Proceedings of the 29th Annual Conference on Liquid Atomization and Spray Systems*, 2017.

[10] Kastengren, A.L., Powell, C.F., Arms, D., Dufresne, E. & Wang, J., Spray diagnostics at the advanced photon source 7-bm beamline. *Proceedings of the 22nd Annual Conference on Liquid Atomization and Spray Systems*, 2010.

[11] Kastengren, A.L. & Powell, C.F., Synchrotron x-ray techniques for fluid dynamics. *Experiments in Fluids*, **55**(3), article 1686, 2014.

[12] Kastengren, A.L., X-ray fluorescence as a gas-phase mixing diagnostic. *Proceedings of the Central States Section of the Combustion Institute Spring Technical Meeting*, 2014.

[13] Donaldson, C.D. & Snedeker, R.S., A study of free jet impingement. Part 1. Mean properties of free and impinging jets. *J. of Fluid Mechanics*, **45**(2), pp. 281–319, 1971.

[14] Crist, S., Sherman, P.M. & Glass, D.R., Study of the highly underexpanded sonic jet. *AIAA Journal*, **4**, pp. 68–71, 1966.

[15] Lewis, C.H. Jr & Carlson, D.J., Normal shock location in underexpanded gas and gas-particle jets. *AIAA Journal*, **2**(4), pp. 776–777, 1964.

[16] Addy, A.L., Effects of axisymmetric sonic nozzle geometry on Mach disk characteristics. *AIAA Journal*, **19**(1), pp. 121–122, 1981.

[17] Lin, K.-C., Bornhoft, B., Kastengren, A. & Carter, C., Derivations of averaged two-phase flow properties using x-ray fluorescence measurements. *AIAA Paper 2018-1547*, 2018.